

Case-Aware Medical Image Classification with Multimodal Knowledge Graphs and Reliability-Guided Refinement

Yiming Xu*

University of Science and Technology
of China
Hefei, China
xym30@mail.ustc.edu.cn

Yixuan Liu*

University of Science and Technology
of China
Hefei, China
lyx1022@mail.ustc.edu.cn

Yuhang Zhang

University of Science and Technology
of China
Hefei, China
yhzhang@mail.ustc.edu.cn

Ling Zheng

University of Science and Technology
of China
Hefei, China
lingzheng@mail.ustc.edu.cn

Yihan Wang

University of Science and Technology
of China
Hefei, China
yihanw@mail.ustc.edu.cn

Qi Song[†]

University of Science and Technology
of China
Hefei, China
qisong09@ustc.edu.cn

Abstract

Deep learning has brought significant progress to medical image classification, yet most existing methods still rely on isolated visual evidence and cannot effectively leverage similar cases or external knowledge. In clinical practice, diagnosis is typically supported by similar historical cases and their associated symptoms. To explicitly model this evidence-based diagnostic process, we propose a case-aware reasoning framework driven by multimodal knowledge graphs for medical image classification. Specifically, we construct a case-aware multimodal knowledge graph as a structured diagnostic memory, where diseases, images, and symptoms are hierarchically organized. Given an input image, our method adaptively retrieves similar cases from this memory and extracts their corresponding case-centered subgraphs. We further introduce a knowledge propagation and injection mechanism, in which an image-centric Graph Attention Network aggregates heterogeneous semantics into case-based features, followed by a bidirectional cross-modal attention mechanism that injects these features into visual representations for cross-modal alignment. To mitigate noisy retrieval, we design a confidence-calibrated decision refinement scheme that estimates the reliability of each retrieved case by jointly considering prediction confidence and sample similarity, and reweights its contribution to the final prediction, providing interpretable case-level evidence. Extensive experiments on multiple medical imaging datasets demonstrate that our approach consistently outperforms strong baselines, while ablation and qualitative analyses validate its effectiveness and interpretability. The code is available at <https://anonymous.4open.science/r/MKG-CARE-8B7B>.

CCS Concepts

• **Computing methodologies** → **Knowledge representation and reasoning.**

Keywords

Medical Image Classification, Multimodal Knowledge Graph, Knowledge Enhancement, Analogical Learning

1 Introduction

Medical image diagnosis constitutes a core pillar of computer-aided diagnosis (CAD) [3, 12, 34], aiming to automatically identify disease-relevant patterns across diverse imaging modalities, including ultrasound [1, 29], gastrointestinal endoscopy [2, 16], computed tomography (CT) [11, 21, 28], and dermatologic imaging [6, 10, 30]. This process is directly tied to early disease screening and precise clinical intervention. While conventional vision-based models [14, 17, 20] (e.g., CNNs, ViTs, and Mamba) have achieved significant progress, they predominantly rely on pixel-level feature extraction, often struggling to capture highly context-dependent pathological patterns. Recently, Large Vision-Language Models (LVLs), such as HealthGPT [15], HuatuoGPT [38], GPT-5.1 [23], and Gemini [5], have demonstrated immense potential in cross-modal reasoning. However, the development of domain-specific foundation models remains heavily constrained by the scarcity of annotated medical data and prohibitive computational costs. Furthermore, such data-driven diagnostic models provide limited evidence traceability and often treat each patient visit as an independent and static event, performing inference solely based on the current imaging input.

To overcome these bottlenecks, incorporating prior knowledge to guide diagnostic reasoning has emerged as a prominent research trend. The first category of methods [8, 39] attempts to leverage the internal parametric knowledge of Large Language Models (LLMs) to generate multi-dimensional prior descriptions for input images. However, constrained by the inherent “hallucination” issue of LLMs, such automatically generated texts often suffer from factual deviations, leading to the injection of unreliable knowledge. The second line of research introduces external structured knowledge via medical Knowledge Graphs (KGs) [9, 35, 41] to provide rigorous medical concepts, improving the factual consistency of diagnostic reasoning. Despite these advances, both paradigms largely confine their priors to generated text or abstract medical concepts, while overlooking the reusable diagnostic experience embedded in historical cases. Real-world clinical diagnosis is inherently an evidence-based and experience-driven process, wherein physicians typically compare similar historical cases to support their final decisions. Motivated by this observation, a third category focuses on case retrieval, recalling similar historical cases as contextual inputs [32] to provide intuitive

*Both authors contributed equally to this research.

[†]Corresponding author.

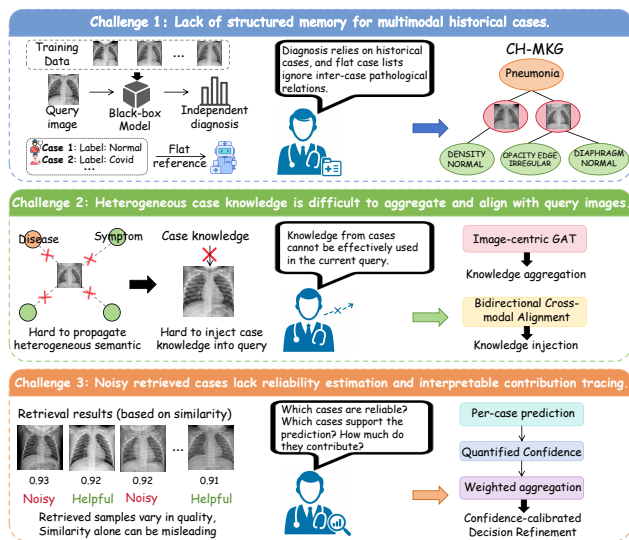


Figure 1: Challenges of medical image diagnosis. Each row follows a consistent three-part layout: the left panel illustrates the problem scenario through visual diagrams; the middle panel contains a textual summary of the core issue within a speech bubble; and the right panel presents the corresponding solution pipeline, thereby establishing a clear challenge-to-solution mapping.

empirical references. As shown in Figure 1, although these attempts mitigate the limitations of purely data-driven models to some extent, establishing a diagnostic framework that truly aligns with clinical reasoning still faces the following three major challenges:

Challenge 1: Lack of structured memory for multimodal historical cases. While referring to historical cases is crucial, most existing methods merely utilize them as training data, implicitly encoding them into model weights. This restricts the inference phase to making independent predictions on isolated query images. Even when recent retrieval-augmented approaches introduce reference samples, they typically treat the retrieved cases as flat, unstructured lists, which severs the lateral connections between cases and overlooks complex pathological correlations. Furthermore, although traditional knowledge graphs attempt to model clinical associations, they are predominantly restricted to text-only medical concepts. This text-only nature not only neglects crucial visual evidence but also makes it exceedingly difficult to cross-modally retrieve relevant structured knowledge directly using visual queries.

Challenge 2: Heterogeneous case knowledge is difficult to aggregate and align with query images. After retrieving similar case subgraphs, effectively bridging the modality gap between continuous visual features and discrete structured semantics emerges as a new technical bottleneck. On the one hand, within a case subgraph, significant representational discrepancies exist between the image entity and its neighboring entities (e.g., symptoms and diseases), hindering the dynamic message passing and semantic aggregation of heterogeneous information. On the other hand, the lack of effective interaction between the current query image

and the retrieved cases makes it difficult to deeply integrate the extracted structured case knowledge into the diagnostic reasoning of the current query.

Challenge 3: Noisy retrieved cases lack reliability estimation and interpretable contribution tracing. Although introducing similar cases can supplement clinical evidence, the quality of retrieved samples varies, and noisy or low-relevance cases can easily mislead the model’s diagnostic direction. Existing retrieval-augmented methods mostly lack mechanisms to quantify the reliability of auxiliary samples, failing to explicitly measure the specific contribution of each historical case to the final prediction. This implicit fusion approach makes it difficult for physicians to clearly trace whether the current prediction is supported or contradicted by specific historical cases, severely limiting the model’s interpretability and trustworthiness in high-risk clinical scenarios.

To address the above challenges, we propose a case knowledge graph-based solution that augments both the data and model levels. **For Challenge 1**, we construct a case-aware hierarchical multimodal knowledge graph (CH-MKG). Specifically, we select representative images from each disease and integrate multi-dimensional, fine-grained symptom annotations provided by clinical experts to construct a “disease-image-symptom” hierarchical graph structure. During the retrieval phase, we design an adaptive contextual retrieval strategy to dynamically define the retrieval boundary by analyzing the similarity gradient between adjacent candidate cases, thereby precisely extracting star-shaped subgraphs with similar images as central entities and associated symptoms and diseases as neighboring nodes. This design effectively filters out interference from low-relevance samples, providing high-quality, structured multimodal prior guidance for the current query image. **For Challenge 2**, we design a case knowledge propagation and injection module (KPI). First, within the case subgraphs, we employ an image-centric Graph Attention Network [33] for explicit message passing, which adaptively aggregates the peripheral symptom and disease semantics into the central image node, generating a structured knowledge representation enriched with clinical context. Subsequently, to achieve deep fusion between the prior knowledge and the current query image, we introduce a dual cross-modal attention mechanism. This mechanism facilitates bidirectional mutual querying and guidance between visual features and knowledge graph, achieving cross-case alignment and deep knowledge injection. **For Challenge 3**, we introduce a Confidence-calibrated Decision Refinement (CDR) module. This module utilizes a second-pass forward inference mechanism to independently evaluate the reliability of each historical case by synthesizing sample similarity and prediction confidence. Subsequently, it performs an adaptive fusion of the prediction distributions based on these reliability weights. This mechanism not only suppresses the interference of retrieval noise but also explicitly characterizes the specific contribution of each auxiliary case to the final decision. In summary, our contributions are as follows:

- We construct a “disease-image-symptom” case-aware hierarchical multimodal knowledge graph and combine it with an adaptive retrieval strategy to precisely extract star-shaped local subgraphs as priors. Concurrently, we design a case knowledge propagation

and injection module. This module dynamically aggregates heterogeneous semantics within the subgraphs and subsequently achieves deep alignment of cross-case features.

- We introduce a Confidence-calibrated Decision Refinement module, endowing the model with high interpretability and robustness. Utilizing a second-pass forward inference mechanism, this module dynamically quantifies the reliability of historical cases by synthesizing sample similarity and prediction confidence, followed by adaptive fusion. This not only effectively mitigates retrieval noise but also explicitly traces the contribution of each auxiliary case to the final diagnosis.
- Extensive quantitative evaluations and qualitative visualization results fully validate the effectiveness of our proposed multimodal knowledge graph and diagnostic framework. The results demonstrate that this method possesses significant advantages in both improving classification performance and enhancing the transparency of the decision-making process.

2 Related Work

2.1 Vision-based methods

A dominant paradigm in medical image classification treats diagnosis as an isolated visual inference problem, where each image is processed independently without external context or historical references. Early approaches are primarily based on convolutional neural networks (CNNs), such as EfficientNet [31] and ConvNeXt [19], which improve performance through architectural scaling and optimization. Transformer-based models, including Swin Transformer [18], further enhance global context modeling by capturing long-range dependencies in medical images. More recently, state-space models such as VMamba [17] and its medical adaptation MedMamba [37] have demonstrated strong efficiency and representation capability for high-resolution medical data. In parallel, large vision-language models (LVLMs), including general-purpose models such as GPT [22] and Gemini [5], as well as medical-domain variants such as HealthGPT [15], HuatuoGPT [38], and MedGemma [27], have shown promising cross-modal reasoning ability by leveraging large-scale pretraining. Despite these advances, such methods fundamentally rely on single-image inference, where knowledge is implicitly encoded in model parameters. This paradigm lacks explicit mechanisms to incorporate similar historical cases or structured clinical knowledge, making it difficult to emulate the experience-driven and evidence-based reasoning process of real-world clinical diagnosis.

2.2 Knowledge-enhanced medical image diagnosis methods

To address the limitations of purely data-driven models, a growing body of work introduces external knowledge or retrieval mechanisms to enhance medical image understanding. One line of research leverages textual knowledge to complement visual features. For example, KEM [39] utilizes LLM-generated symptom descriptions as semantic knowledge to guide medical image classification. Another line of research incorporates structured knowledge graphs to inject domain knowledge into vision-related tasks. Methods such as KG-CMI [41] integrate text-only knowledge graphs via embedding modules, enabling alignment between lesion features

and medical concepts. However, these approaches typically construct text-centric knowledge graphs, where visual information is not explicitly represented as graph nodes. Consequently, the interaction between image evidence and knowledge remains indirect, limiting the directness of knowledge grounding in visual reasoning. A third line of research introduces retrieval-based methods that leverage similar historical cases as auxiliary evidence. Representative works such as ECG-Doctor [32] retrieve clinically similar samples and use them to support prediction via in-context learning. Recently, RareAgents [4] further extends retrieval-based reasoning to rare disease diagnosis and medication recommendation, which retrieves similar phenotypic cases and longitudinal patient records as dynamic long-term memory to enhance multi-disciplinary agent decision-making. However, these methods generally organize retrieved cases as flat lists without explicitly modeling the structural relationships among cases. Consequently, they fail to capture structured dependencies and lack transparency in how retrieved cases influence the final decision.

3 Method

3.1 Overview

As illustrated in Figure 2, our framework takes a query image as input and produces a final prediction P_{final} through three stages. In the Case-aware Hierarchical Multimodal Knowledge Graph (CH-MKG) module, a vision encoder extracts visual features from the query image, which are used to adaptively retrieve relevant similar images. These retrieved images, along with their associated disease and symptom nodes, form a structured multimodal knowledge graph that organizes case-aware knowledge hierarchically. Next, in the Knowledge Propagation and Injection (KPI) module, an image-centric graph attention mechanism propagates information across image, symptom, and disease nodes to produce enriched knowledge features. These features are then aligned with the query visual feature via bidirectional cross-modal attention, and the resulting fused representation is fed to a classifier to produce an initial prediction P_q . Finally, in the Confidence-calibrated Decision Refinement (CDR) module, each retrieved similar case is passed through the same pipeline to obtain its prediction P_i . The module aggregates these predictions by considering both their similarity and their confidence, yielding an auxiliary distribution P_{sim} . This is adaptively fused with P_q to obtain the final P_{final} . Thus, the model moves from isolated visual inference to case-aware reasoning with explicit utilization of historical similar cases and decision refinement.

3.1.1 Case-aware Knowledge Graph Construction. To simulate how clinicians reason by referring to prior experience with similar historical cases, we construct a case-aware hierarchical multimodal knowledge graph tailored to each dataset, serving as a clinician’s memory bank. Specifically, we select representative image samples for each disease, which serve as image nodes in the graph. Each image node is then connected to its corresponding disease node and the associated symptom nodes derived from expert annotations. Edges encode two types of relations: image-disease associations indicating class membership, and image-symptom associations capturing observable clinical characteristics.

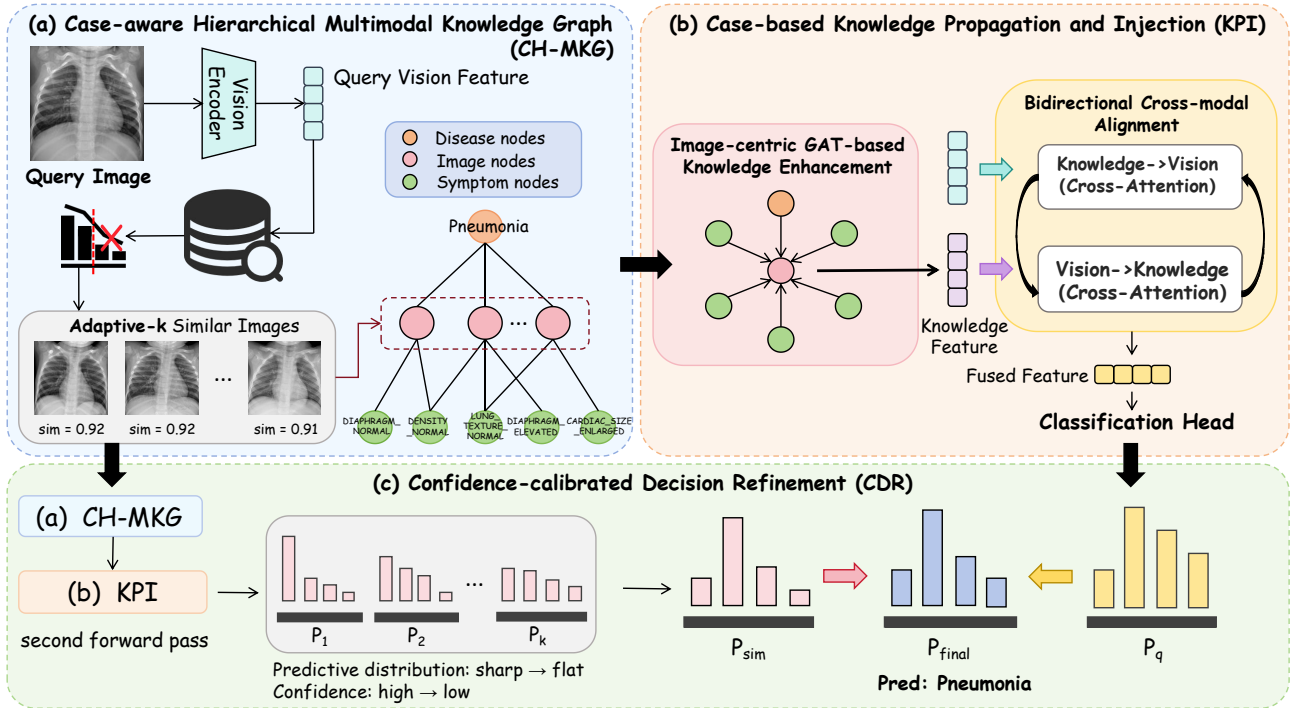


Figure 2: The overall framework of MKG-CARE consists of three modules: (a) Case-aware Hierarchical Multimodal Knowledge Graph, (b) Knowledge Propagation and Injection, (c) Confidence-calibrated Decision Refinement.

This forms a hierarchical multimodal knowledge graph organized from top to bottom: the top layer consists of disease nodes representing diagnostic classes, serving as semantic anchors; the middle layer consists of image nodes representing representative cases associated with each disease; and the bottom layer consists of symptom nodes representing fine-grained clinical attributes that describe visual patterns. This hierarchical design enables bidirectional information flow: disease nodes at the top propagate global semantic guidance downward, while symptom nodes at the bottom transmit fine-grained descriptive evidence upward. Such a multi-granularity organization enables structured reasoning by explicitly modeling the relationships among categories, cases, and clinical symptoms. Compared with text-only knowledge graphs, our formulation explicitly incorporates visual instances as entities, allowing tighter coupling between image features and medical knowledge.

3.1.2 Adaptive Case Retrieval. Given a query image, we first encode it into a feature vector using a pre-trained MedMamba [37] encoder. We then retrieve similar image nodes from a FAISS vector database, which is constructed offline using the representative image nodes extracted from the training set. Instead of using a fixed number of retrievals, we adopt an adaptive retrieval strategy [40] that determines the effective number of relevant cases per query. Specifically, let S_i denote the similarity score of the i -th retrieved

image node. We compute a similarity ratio as follows:

$$u_i = \log \left(\frac{S_i}{S_{i+1}} \right), i \in \{1, 2, \dots, k-1\} \quad (1)$$

When u_i exceeds a predefined threshold u_{th} , it indicates a sharp drop in similarity. We therefore truncate the retrieval list at position i , retaining only the most informative cases while filtering out noisy or weakly related samples.

After selecting the image nodes, we construct a query-specific subgraph by performing a one-hop expansion over the knowledge graph, incorporating connected symptom and disease nodes. This results in an informative image-centric subgraph that consists of the retrieved similar cases and their associated symptom and disease nodes, serving as a structured knowledge context for subsequent knowledge feature extraction.

This retrieval-and-expansion mechanism transforms the input from an isolated sample into a structured reasoning unit, thereby enabling the model to reason by referring to similar cases and leveraging their associated semantic knowledge.

3.2 Knowledge Propagation and Injection

After constructing the retrieval subgraph, our goal is to effectively leverage it as a structured knowledge context to obtain concise knowledge representations of similar cases. To this end, we design a two-stage knowledge propagation and injection mechanism that first performs image-centric Graph Attention Network-based

knowledge enhancement over the retrieval subgraph, and then conducts bidirectional cross-modal alignment between the resulting knowledge representation and the query visual features. This design enables cross-modal semantic enrichment and deep cross-case interaction, allowing visual evidence to be jointly interpreted with structured clinical knowledge.

3.2.1 Image-centric Graph Attention Network-based Knowledge Enhancement. We first perform message passing over the retrieval subgraph using a two-layer image-centric Graph Attention Network [33]. Let $\mathbf{h}_i^{(l)}$ denote the representation of node i at layer l . The node features are initialized as follows: image nodes are initialized with MedMamba [37] embeddings, while symptom and disease nodes are initialized using BioBERT [13]. The GAT layer updates node representations by aggregating information from their neighbors with attention weights:

$$\mathbf{h}_i^{(l+1)} = \sigma \left(\sum_{j \in \mathcal{N}(i)} \alpha_{ij}^{(l)} \mathbf{W}^{(l)} \mathbf{h}_j^{(l)} \right), \quad (2)$$

where $\alpha_{ij}^{(l)}$ is the attention coefficient computed as:

$$\alpha_{ij}^{(l)} = \frac{\exp \left(\text{LeakyReLU} \left(\mathbf{a}^{(l)\top} \left[\mathbf{W}^{(l)} \mathbf{h}_i^{(l)} \parallel \mathbf{W}^{(l)} \mathbf{h}_j^{(l)} \right] \right) \right)}{\sum_{k \in \mathcal{N}(i)} \exp(\cdot)}. \quad (3)$$

Through two stacked GAT layers, information is propagated along the structure of the graph. This process enables retrieved image nodes to absorb medical semantics from symptom and disease nodes, while knowledge nodes simultaneously aggregate statistical evidence from multiple similar images, allowing the model to assign higher attention weights to symptoms that are more discriminative for classification, effectively amplifying their contribution while suppressing noisy symptom nodes. As a result, each retrieved image node is transformed into a knowledge-enhanced representation that integrates both visual similarity and semantic context.

To obtain a compact knowledge representation, we aggregate the enhanced representations of retrieved images into a single vector. Specifically, we compute similarity-aware weights based on the query embedding and perform normalized weighted aggregation:

$$\mathbf{z}_{kg} = \sum_{i=1}^K \tilde{w}_i \mathbf{h}_i^{(L)}, \quad \tilde{w}_i = \frac{\text{sim}_i}{\sum_j \text{sim}_j}, \quad (4)$$

where sim_i denotes the similarity between the query and the i -th retrieved image. This aggregated vector \mathbf{z}_{kg} captures knowledge-aware evidence from multiple related cases, serving as a global knowledge representation for subsequent alignment.

3.2.2 Bidirectional Cross-modal Alignment. While the graph propagation stage aggregates textual semantics into the visual features of similar images to obtain knowledge-enhanced representations, it does not explicitly align the knowledge feature space with the query visual feature space. To bridge this gap, we design a two-layer bidirectional cross-modal attention module, where each layer consists of a CrossModalBlock with bidirectional interactions.

Given the query visual feature $\mathbf{v}_q \in \mathbb{R}^d$ and the knowledge representation $\mathbf{z}_{kg} \in \mathbb{R}^d$, each CrossModalBlock performs the following sequence of operations to enable interaction between them.

First, we update the knowledge representation conditioned on the query feature as context:

$$\mathbf{z}_{kg}^{(1)} = \text{MHA}(\mathbf{Q} = \mathbf{z}_{kg}, \mathbf{K} = \mathbf{v}_q, \mathbf{V} = \mathbf{v}_q), \quad (5)$$

which allows the knowledge vector to incorporate visual evidence from the query image.

Next, we update the query representation using the newly updated knowledge feature:

$$\mathbf{v}_q^{(1)} = \text{MHA}(\mathbf{Q} = \mathbf{v}_q, \mathbf{K} = \mathbf{z}_{kg}^{(1)}, \mathbf{V} = \mathbf{z}_{kg}^{(1)}), \quad (6)$$

enabling the visual representation to be explicitly guided by semantically enriched knowledge.

Updates are followed by residual connections and normalization.

$$\mathbf{z}_{kg} = \text{LayerNorm}(\mathbf{z}_{kg} + \mathbf{z}_{kg}^{(1)}), \mathbf{v}_q = \text{LayerNorm}(\mathbf{v}_q + \mathbf{v}_q^{(1)}), \quad (7)$$

and further refined by modality-specific MLP layers:

$$\mathbf{z}_{kg} = \text{LayerNorm}(\mathbf{z}_{kg} + \text{MLP}_{kg}(\mathbf{z}_{kg})), \quad (8)$$

$$\mathbf{v}_q = \text{LayerNorm}(\mathbf{v}_q + \text{MLP}_{img}(\mathbf{v}_q)). \quad (9)$$

We stack two such CrossModalBlocks to enable iterative interaction between modalities. This bidirectional design ensures that knowledge features are grounded in visual evidence, while visual features are semantically enriched by knowledge, leading to a well-aligned joint representation space.

Finally, we construct a fused representation by combining complementary information from both modalities. Specifically, we use four types of feature interactions:

$$\mathbf{h}_{fusion} = \text{concat}(\mathbf{v}_q, \mathbf{z}_{kg}, |\mathbf{v}_q - \mathbf{z}_{kg}|, \mathbf{v}_q \odot \mathbf{z}_{kg}), \quad (10)$$

where the absolute difference captures discrepancies, and element-wise product captures consistency between modalities.

The fused representation is then fed into a classification head:

$$\text{logits}_q = \text{MLP}(\mathbf{h}_{fusion}), \quad (11)$$

which produces the initial prediction for the query image.

3.3 Confidence-calibrated Decision Refinement

Although retrieval provides additional evidence, the quality of retrieved samples varies, and noisy cases can mislead the model's diagnostic direction. Relying solely on similarity to the query is often insufficient, as highly similar cases may still be mislabeled or contain clinically irrelevant features, making similarity alone an unreliable indicator of sample reference value. Moreover, existing retrieval-augmented methods [32] lack mechanisms to quantify the contribution of each similar case to the final decision, making it difficult to interpret how the retrieved evidence influences the prediction and to understand the rationale behind the final decision.

To address these issues, we design a confidence-calibrated decision refinement mechanism that performs a second-pass inference over the retrieved cases, quantifying the reliability of each sample based on both its similarity to the query and its prediction confidence. These reliability weights are then used to fuse the retrieved predictions with the query result, thereby suppressing retrieval noise. Meanwhile, the confidence of similar cases provides an interpretable basis for understanding the final prediction, offering both robustness and interpretability.

We first obtain the initial prediction for the query image based on the query itself. Next, for each retrieved similar sample, we reuse its pre-constructed subgraph and perform the same forward inference pipeline to obtain its prediction distribution. The two prediction distributions are formulated as:

$$\mathbf{P}_q = \text{softmax}(\text{logits}_q), \mathbf{P}_i = \text{softmax}(\text{logits}_i), \quad (12)$$

where \mathbf{P}_q denotes the baseline prediction of the query image and \mathbf{P}_i denotes the prediction distribution of each retrieved sample.

To assess the reliability of each retrieved sample, we define its prediction confidence as:

$$c_i = \max(\mathbf{P}_i), \quad (13)$$

which reflects the certainty of its prediction.

We compute the contribution weight of each retrieved sample by jointly considering its similarity to the query and its prediction confidence. Specifically, the weight is defined as:

$$w_i \propto (\text{sim}_i)^\alpha \cdot (c_i)^\beta, \quad (14)$$

where α and β are hyperparameters that control the relative importance of similarity and confidence, respectively.

Based on these weights, we aggregate the predictions of retrieved samples into a unified distribution:

$$\mathbf{P}_{sim} = \frac{\sum_i w_i \mathbf{P}_i}{\sum_i w_i}. \quad (15)$$

Finally, we combine the query prediction and the aggregated prediction from retrieved samples:

$$\mathbf{P}_{final} = (1 - \lambda)\mathbf{P}_q + \lambda\mathbf{P}_{sim}, \quad (16)$$

and the final predicted label is obtained by $\arg \max(\mathbf{P}_{final})$.

This refinement mechanism improves robustness by emphasizing reliable and relevant retrieved samples, while suppressing noisy ones. Besides, the weighting scheme provides a quantitative measure of how each retrieved case contributes to the final decision, enhancing the interpretability in a case-based reasoning manner.

4 Experiments

4.1 Experimental Setup

4.1.1 Datasets. We evaluate our method on five widely-used medical image classification benchmarks: BreastMNIST [1], DermaMNIST [36], Kvasir [25], PAD_UFES_20 [24], and RetinaMNIST [36], spanning dermatology, ophthalmology, pathology, and gastrointestinal imaging. These datasets vary in class granularity, data distribution, and visual complexity, exhibiting challenges such as class imbalance, fine-grained visual differences, and high intra-class variation, which together provide a comprehensive testbed for evaluating generalization, robustness, and knowledge-enhanced reasoning. We summarize the five datasets and the corresponding knowledge graph scales (number of entities and edges) in Table 1.

4.1.2 Implementation Details. Our experiments are conducted using PyTorch on an NVIDIA RTX A800 GPU. For fair comparison, all input images are resized to $224 \times 224 \times 3$. For efficient retrieval, representative image features are indexed using FAISS.

Table 1: Summary of five medical image classification datasets and corresponding knowledge graph scales.

Dataset	Domain	Classes	Size	KG Entities	KG Edges
BreastMNIST	Pathology	2	780	60	271
DermaMNIST	Dermatology	7	10,015	163	1088
Kvasir	Gastrointestinal	8	8,000	162	984
PAD_UFES_20	Dermatology	6	2,298	153	1000
RetinaMNIST	Ophthalmology	5	1,600	106	1040

The knowledge-aware feature propagation module uses a two-layer Graph Attention Network with multi-head attention. Specifically, each layer employs 4 attention heads, and the hidden dimension is fixed at 768. A dropout rate of 0.2 is applied within the attention mechanism to mitigate overfitting. For cross-modal interaction, we employ a two-layer bidirectional CrossModalBlock. Each layer consists of multi-head cross-attention with 4 heads, an embedding dimension of 768, and an attention dropout rate of 0.2. This is followed by residual connections, LayerNorm, and modality-specific MLPs. Each MLP is implemented as a two-layer feed-forward network with ReLU activation. A dropout rate of 0.4 is applied for further refinement within each modality.

After cross-modal alignment, we construct a fused representation by combining the query visual feature and knowledge feature, resulting in a 4×768 -dimensional vector. This fused feature is then fed into a two-layer MLP classifier with ReLU activation and dropout (0.4) to produce the final logits, and the model is trained using cross-entropy loss.

For optimization, we use the AdamW optimizer with an initial learning rate of 5×10^{-5} and weight decay of 0.02. A StepLR scheduler is applied with step size 25 and decay factor 0.5 to ensure stable convergence. The model is trained with a batch size of 64 for up to 40 epochs, with early stopping based on validation performance to prevent overfitting. Gradient clipping is applied to stabilize optimization. For the confidence-calibrated refinement module, the weighting hyperparameters are set to $\alpha = 1$ and $\beta = 1$ by default.

4.1.3 Baselines. To evaluate the proposed method, we compare it with diverse baselines spanning multiple paradigms, including conventional vision-based architectures, large multimodal models (both general-purpose and medical-specific), and knowledge-enhanced approaches. Specifically, we include several representative **vision-based deep learning models**, such as Swin-Transformer [18], EfficientNetV2 [31], ConvNeXt [19], and VMamba [17], which are widely used for medical image classification. We also report the performance of MedMamba [37] as a backbone baseline to verify the improvement brought by our knowledge-enhanced framework. For **large multimodal models**, we evaluate both general-purpose baselines including GPT-5.1 [23], Gemini-3-pro [7], and Qwen3.5-plus [26], as well as medical-specific models such as HealthGPT [15], HuatuoGPT [38], and MedGemma [27], which are designed for healthcare applications. These models leverage large-scale multimodal pretraining and demonstrate strong generalization capability. Furthermore, we compare with a recent **knowledge-enhanced method** KEM [39] that incorporates textual knowledge generated by large language models into visual classification, serving as a

reference for evaluating structured knowledge integration. This diverse set of baselines ensures a fair and comprehensive comparison across different modeling paradigms.

4.1.4 Evaluation Metrics. We evaluate all methods using two widely adopted metrics for medical image classification: Overall Accuracy (OA) and Macro-AUC. OA measures the proportion of correctly classified samples, reflecting general prediction performance. However, in medical datasets with imbalanced class distributions, OA alone may not fully capture the model’s ability to distinguish different disease categories. Therefore, we additionally report Macro-AUC, which computes the average area under the ROC curve across all classes, treating each class equally. This metric captures per-class discriminative capability, providing a more comprehensive evaluation especially for rare or underrepresented classes. Together, these two metrics offer a balanced assessment of both overall performance and class-wise robustness.

4.2 Main Results

4.2.1 Overall Performance. Table 2 reports the comparison results of all methods on five medical image classification benchmarks. We evaluate all methods using Overall Accuracy (OA) and AUC, comparing our approach against a comprehensive set of baselines, including vision-based models, medical/general Large Vision-Language Models (LVLMs), and knowledge-enhanced methods.

Overall, our method achieves the best OA performance on all five datasets and the best AUC on four of them, demonstrating consistent performance gains across diverse medical domains and classification settings. These results validate the effectiveness of case-aware reasoning in medical image classification.

Notably, while achieving the highest OA on BreastMNIST, our method yields the second-best Macro-AUC. This is attributed to the dataset’s artificially merged binary structure. Specifically, our model’s fine-grained semantic disentanglement inadvertently separates samples within the heterogeneous negative class (merged from normal and benign), which slightly affects ranking-based metric AUC without compromising the final classification decisions.

4.2.2 Comparison with Vision-based Models. Compared to conventional vision architectures (e.g., EfficientNetV2, Swin-Transformer, ConvNeXt, and VMamba), our method achieves consistent improvements. These baselines rely purely on visual features and often struggle with the high intra-class variation common in medical imaging. More importantly, our approach significantly outperforms MedMamba [37], which serves as our visual backbone. This demonstrates that our performance gains are not merely derived from a stronger encoder, but primarily from the effective integration of structured knowledge and similar-case reasoning.

4.2.3 Comparison with LVLMs. We further compare with medical-specific (Health-GPT, MedGemma, HuatuoGPT) and general-purpose (GPT-5.1, Gemini-3, Qwen3.5-plus) LVLMs. While these billion-parameter models possess strong general capabilities, they often lack stability in specialized medical scenarios requiring fine-grained visual perception. Furthermore, they incur substantial computational cost. In contrast, our method maintains a computationally efficient architecture. By explicitly grounding predictions in retrieved cases and structured knowledge, our approach provides

more reliable and domain-aware representations, outperforming large-scale LVLMs while remaining computationally efficient.

4.2.4 Comparison with Knowledge-enhanced Method. Compared to the knowledge-enhanced baseline KEM [39], our method exhibits consistent superiority. KEM processes images in isolation and relies on LLM-generated symptom descriptions, which lack structural hierarchy and are prone to hallucinations. Our framework overcomes these limitations through three key designs: (1) we retrieve and reason over historical similar cases rather than performing isolated inference; (2) we utilize expert-annotated medical knowledge, eliminating hallucination risks; and (3) we construct a structured graph with an attention mechanism, enabling the model to dynamically prioritize informative symptoms over noisy ones. Collectively, these advantages lead to our leading performance.

4.3 Ablation Study

We conduct ablation studies on the Kvasir and RetinaMNIST datasets to systematically evaluate the contribution of each core module in our framework: the Case-aware Hierarchical Multimodal Knowledge Graph (CH-MKG), Knowledge Propagation and Injection (KPI), and Confidence-calibrated Decision Refinement (CDR). As shown in Table 3, we adopt a *progressive removal* strategy, starting from the full model and successively disabling individual modules to analyze their impact on overall accuracy (OA).

4.3.1 Impact of the CDR Module. Removing CDR leads to an OA drop on both datasets (Kvasir: 84.0 \rightarrow 83.6; RetinaMNIST: 58.8 \rightarrow 58.0). This degradation highlights CDR’s role in enhancing prediction reliability. By explicitly weighting retrieved cases based on a combination of similarity and confidence, it effectively mitigates the influence of noisy or misleading samples. This demonstrates that confidence-aware case aggregation is essential for robust case-based reasoning, especially when retrieval quality varies.

4.3.2 Impact of the KPI Module. Further disabling KPI causes a more pronounced decline (Kvasir: 83.6 \rightarrow 82.7; RetinaMNIST: 58.0 \rightarrow 56.3). Without KPI, the model degenerates into naive similarity-weighted aggregation and shallow feature concatenation. This indicates that without proper knowledge propagation, the model fails to leverage case-level semantic knowledge and instead relies on superficial feature matching. This demonstrates that KPI is essential for deep cross-modal alignment and propagating textual medical semantics into visual representations.

4.3.3 Impact of the CH-MKG Module. Next, we further disable the CH-MKG module (w/o. CH-MKG & KPI & CDR), where a portion of informative nodes (including representative image nodes and associated symptom nodes) is removed from the knowledge graph. This results in additional performance decline (Kvasir: 82.7 \rightarrow 82.0; RetinaMNIST: 56.3 \rightarrow 56.0), indicating that the effectiveness of the framework is tightly coupled with the availability of high-quality, semantically meaningful nodes. By removing these nodes, the retrieved subgraph becomes less informative, weakening both the case-level evidence provided by similar images and the complementary clinical semantics introduced by symptom nodes. This

Table 2: Performance comparison on five medical image classification benchmarks. All results are reported as OA and AUC, where AUC denotes Macro-AUC for multi-class datasets. The best results are highlighted in bold, and the second-best results are underlined. Rows shaded in gray and blue indicate the knowledge-enhanced method and ours, respectively.

Model	BreastMNIST		DermaMNIST		Kvasir		PAD_UFES_20		RetinaMNIST	
	OA	AUC	OA	AUC	OA	AUC	OA	AUC	OA	AUC
Vision-based										
Swin-Transformer (2021)	75.6	78.8	77.8	93.8	75.2	97.0	59.7	82.5	53.5	72.5
EfficientNetV2 (2021)	84.0	76.4	75.1	90.1	76.3	96.3	51.7	74.1	51.3	70.5
ConvNeXt (2022)	83.3	81.7	67.0	91.9	72.5	96.6	49.4	77.7	51.8	69.8
VMamba (2024)	82.1	80.4	70.3	89.0	69.8	96.2	52.3	82.6	52.3	73.2
MedMamba (2024)	85.3	82.5	77.9	91.7	79.3	<u>97.6</u>	58.8	80.8	54.3	74.7
Med-LVLM										
Health-GPT-XL32 (2024)	37.2	56.3	33.3	52.1	34.5	62.6	39.2	61.9	40.3	49.9
HuatuogPT-Vision-34B (2024)	35.3	55.0	61.7	65.0	47.3	69.9	54.9	65.3	36.5	60.0
medgemma-1.5-4b-it (2026)	73.7	51.2	54.9	60.6	29.2	59.8	53.5	69.5	51.0	62.3
General LVLM										
GPT-5.1 (2025)	64.7	70.9	72.7	84.3	80.3	85.2	57.7	74.2	28.5	48.3
Gemini-3-pro (2025)	80.1	77.6	75.6	85.9	81.6	87.1	61.1	70.7	31.5	58.0
Qwen3.5-plus (2026)	75.0	72.4	56.4	71.9	63.4	79.1	59.1	72.4	47.0	55.7
Knowledge-enhanced										
KEM (2025)	<u>86.5</u>	90.9	<u>81.7</u>	<u>95.8</u>	<u>82.3</u>	97.5	<u>62.0</u>	<u>82.6</u>	<u>55.8</u>	<u>75.6</u>
Ours										
MKG-CARE	87.2	<u>83.1</u>	83.6	96.1	84.0	98.4	62.3	83.3	58.8	76.0

Table 3: Ablation study of key components. We report overall accuracy (OA) on the Kvasir and RetinaMNIST datasets. CH-MKG, KPI, and CDR denote the three modules introduced in our method.

Models	Kvasir	RetinaMNIST
	OA	OA
Full Model	84.0	58.8
w/o. CDR	83.6	58.0
w/o. KPI & CDR	82.7	56.3
w/o. CH-MKG & KPI & CDR	82.0	56.0

observation confirms that our framework does not merely leverage the graph structure, but fundamentally relies on the semantic content encoded in carefully constructed multimodal nodes.

4.4 Case Study

4.4.1 Visualization of Confidence Calibration with Knowledge Graph Reasoning. Figure 3 illustrates our model’s interpretable decision-making process using a Kvasir case. As shown in Figure 3(a), the initial prediction P_q incorrectly favors class 3 over the ground truth (class 6). However, by aggregating retrieved cases via the CDR module, the intermediate prediction P_{sim} successfully shifts toward the

correct class. Figure 3(b) details this mechanism within the knowledge graph, where retrieved similar image nodes are connected to disease nodes and symptom nodes. Symptom nodes are visualized with varying color intensity, reflecting their learned importance during knowledge propagation—higher intensity indicates greater diagnostic reference value in the decision-making process. While multiple retrieved cases exhibit high visual similarity, the CDR module dynamically weights them based on their prediction confidence. Case 1, possessing both high similarity and high confidence for class 6, dominates the refinement process. Conversely, cases with conflicting or uncertain predictions are dynamically down-weighted despite high similarity. This effectively filters retrieval noise and demonstrates how case-based reasoning rectifies uncertain predictions in practice.

4.4.2 Lesion-aware Attention Visualization. Figure 4 uses Grad-CAM to compare the visual reasoning of our method against the MedMamba baseline across five datasets. Consistently, MedMamba produces diffuse attention maps, often highlighting irrelevant background areas or completely missing subtle pathological cues (e.g., Case 4). By contrast, our retrieval-augmented framework generates highly concentrated and semantically accurate activations. It precisely localizes clinically critical regions across diverse domains, such as the hypoechoic mass with irregular margins in ultrasound (Case 1), heterogeneous pigmentation in dermoscopy (Cases 2 and

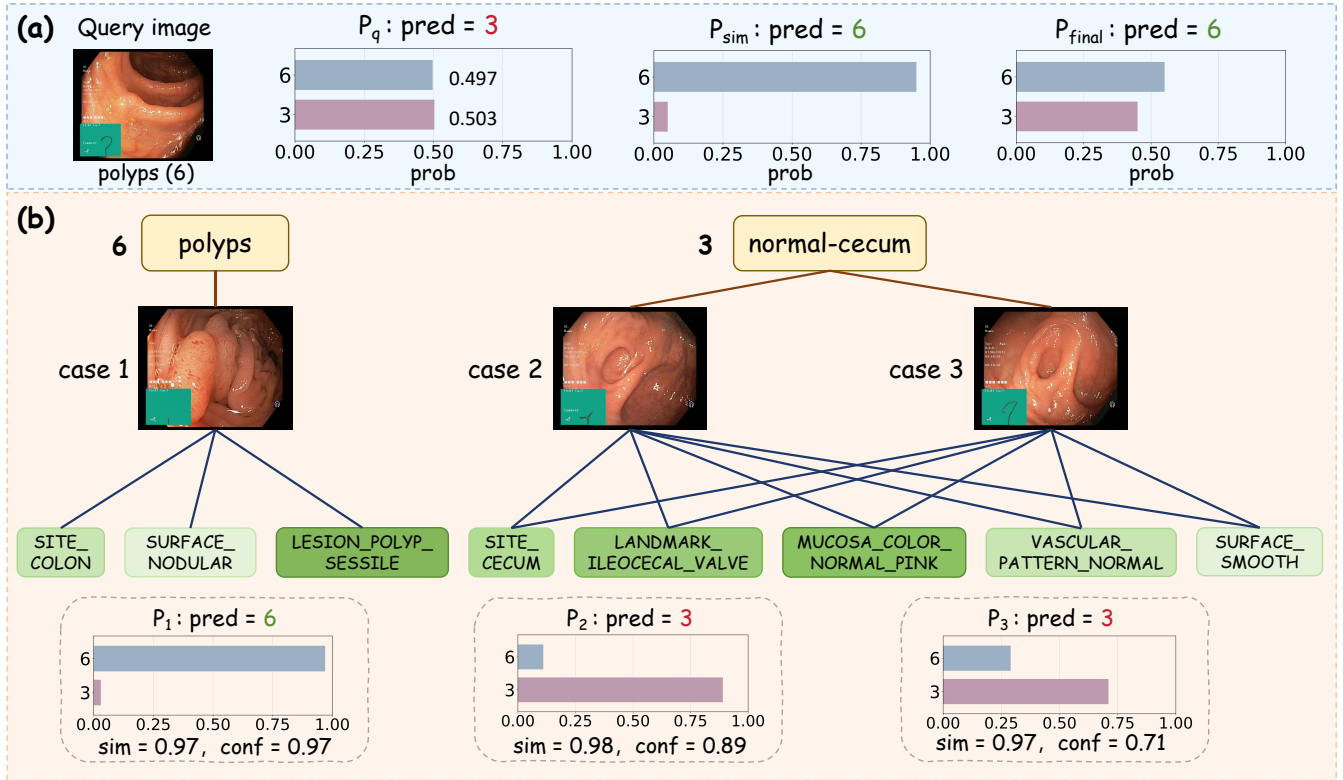


Figure 3: Visualization of confidence calibration with knowledge graph reasoning on the Kvasir dataset. (a) Prediction evolution of the query image from the initial prediction P_q to the retrieved-case aggregated prediction P_{sim} and the final refined prediction P_{final} . (b) Retrieved case-aware hierarchical multimodal knowledge graph, showing the relationships among disease nodes, retrieved image nodes, and symptom nodes. The color intensity of symptom nodes reflects their learned importance during knowledge propagation. Each retrieved case is annotated with its individual prediction distribution, similarity score and prediction confidence, illustrating how the CDR module estimates the reliability of retrieved samples during decision refinement.

4), and specific pathological structures in endoscopy and fundus imaging (Cases 3 and 5). Furthermore, the attention patterns on the query images closely align with those on the retrieved similar cases. This provides strong qualitative evidence that our model effectively transfers cross-case visual knowledge, utilizing analogous disease patterns to refine its lesion focus.

4.5 Further Analysis

4.5.1 Impact of GAT Layers in KPI. We further analyze the influence of the number of GAT layers in the KPI module, with results illustrated in Figure 5(a).

With 0 layers, the model degenerates into a visual-only retrieval baseline without textual knowledge, yielding the lowest performance (0.825 on DermaMNIST and 0.822 on Kvasir). This indicates that relying solely on visual similarity is insufficient for capturing clinically meaningful semantics. Performance improves with 1 layer and peaks at 2 layers (0.836 and 0.840, respectively). Unlike single-layer propagation where knowledge nodes lack cross-case aggregation, the 2-layer GAT optimally facilitates bidirectional message passing: knowledge nodes first aggregate statistical evidence from

multiple images, and then propagate enriched, cross-case semantics back to the image representations. However, further increasing the depth to 3 layers causes a slight performance drop (0.828 / 0.825), primarily due to the well-known over-smoothing effect in graph networks, which weakens node distinctiveness. Therefore, we adopt a 2-layer architecture to balance effective knowledge aggregation and noise control.

4.5.2 Impact of Fusion Coefficient λ in CDR. We also investigate the effect of the fusion coefficient λ in the CDR module, which controls the contribution of retrieved-case predictions P_{sim} in refining the initial query prediction P_q .

As shown in Figure 5(b), different datasets exhibit distinct sensitivity patterns to this parameter. On PAD_UFES_20, the best performance is achieved at a relatively small coefficient ($\lambda = 0.1$, OA = 0.623), and performance gradually decreases as λ increases. This is consistent with the nature of this dataset, where classes are well-separated. In such a setting, the evidence directly available from the query is already sufficiently reliable; incorporating additional information from retrieved cases offers little benefit and may instead

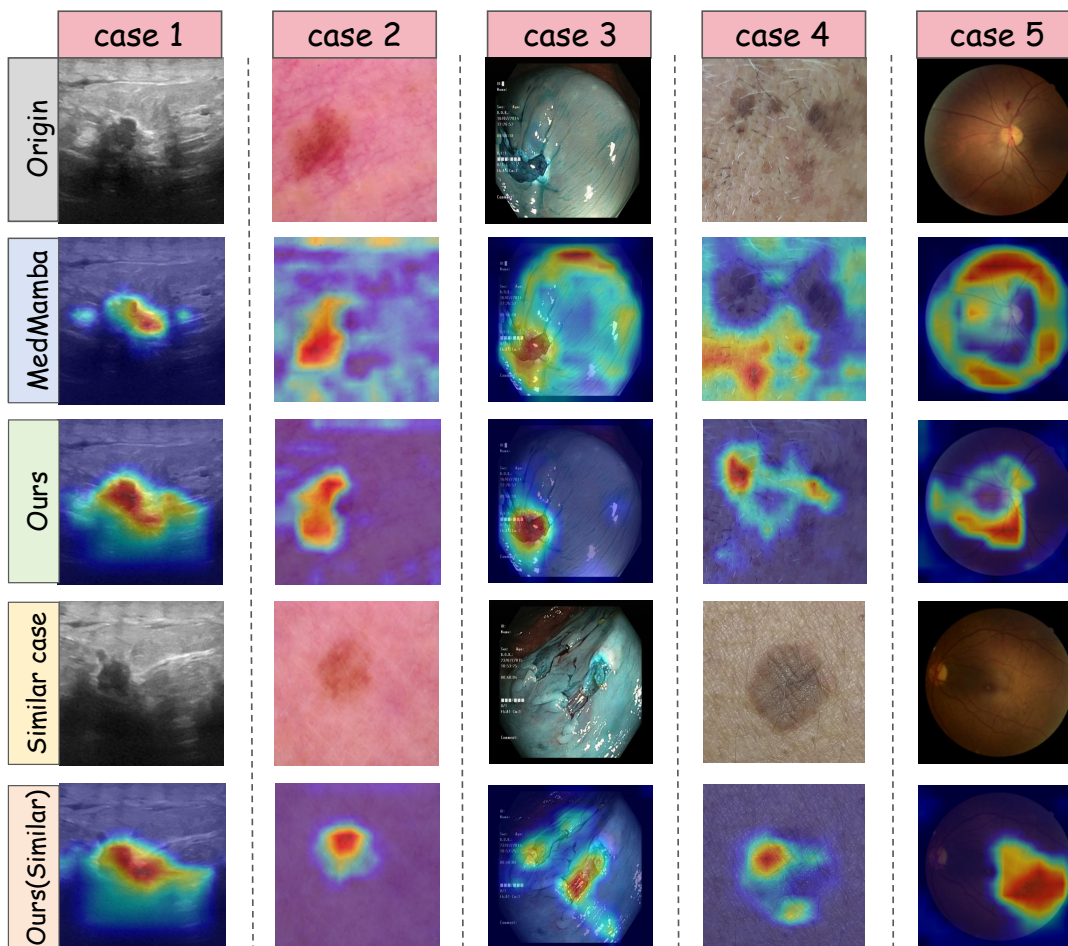


Figure 4: Grad-CAM visualization across five datasets (Case 1–5 correspond to BreastMNIST, DermaMNIST, Kvasir, PAD_UFES_20, and RetinaMNIST, respectively). From top to bottom: original image, MedMamba attention map, our method’s attention map, most similar retrieved image, and our method’s attention map on the retrieved image.

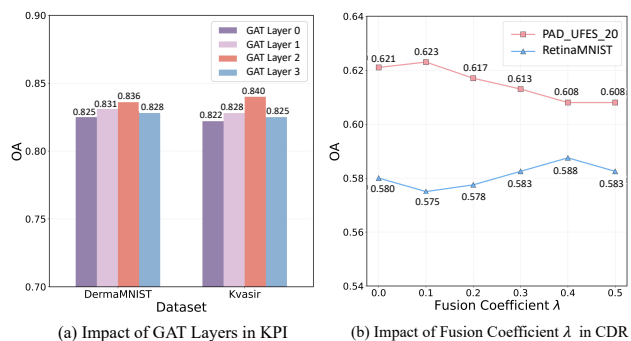


Figure 5: Parameter Sensitivity Analysis of MKG-CARE.

introduce noise. In contrast, RetinaMNIST presents a more challenging scenario. It is essentially a disease grading task, where the

image differences between different grades are very subtle, requiring the model to have fine-grained discrimination capabilities. This naturally leads to blurred boundaries between different categories. Moreover, the retrieved cases themselves are often unreliable—even when their similarity scores seem reasonable. Performance improves steadily as λ increases from 0.0 to 0.4 (from 0.580 to 0.588), before slightly declining at $\lambda = 0.5$. This trend reflects that under such ambiguity and unreliable retrieval, the evidence directly from the query is often insufficient. Here, information from retrieved cases—particularly when weighted by confidence—provides a more robust complement. However, when λ becomes too large, even less reliable retrieved cases begin to dominate, leading to a performance drop beyond the optimal point. Overall, these observations highlight that λ serves as a critical balancing factor between the evidence carried directly by the query and the auxiliary information from retrieved cases. An appropriate setting allows the model to benefit from retrieval-based reasoning where needed, while remaining robust when the query itself is already sufficiently informative.

5 Conclusion

In this paper, we propose MKG-CARE, a framework that performs case-aware reasoning using multimodal knowledge graphs for explainable medical image diagnosis. Unlike conventional approaches that rely on isolated visual inference or flat retrieval, our method constructs a case-aware hierarchical multimodal knowledge graph (CH-MKG) that jointly organizes image, symptom, and disease information in a structured manner. Building upon this representation, we introduce a knowledge propagation and injection module (KPI) that enables image-centric semantic aggregation through graph attention and cross-modal alignment, allowing structured clinical semantics to interact with visual evidence. Furthermore, a confidence-calibrated decision refinement (CDR) mechanism is designed to explicitly quantify the reliability of retrieved cases and adaptively adjust their contributions to the final prediction, improving both robustness and interpretability. Extensive experiments across multiple medical datasets demonstrate consistent performance gains, while qualitative analyses reveal that our model provides structured reasoning paths, case-level evidence attribution, and anatomically meaningful attention, collectively underscoring its potential for deployment in real-world clinical workflows. Overall, this work highlights the importance of integrating multimodal structured knowledge and case-based reasoning, offering a more interpretable and clinically aligned paradigm for medical image diagnosis. In future work, we plan to extend the proposed framework to more complex 3D medical imaging scenarios, such as CT and MRI, where structured multimodal knowledge may further support volumetric evidence modeling and clinically grounded diagnosis.

GenAI Usage Disclosure

During the preparation of this work, the authors used ChatGPT¹ to polish the paper and subsequently reviewed and edited the content. They take full responsibility for the final publication.

References

- [1] Walid Al-Dhabyani, Mohammed Gomaa, Hussien Khaled, and Aly Fahmy. 2020. Dataset of breast ultrasound images. *Data in brief* 28 (2020), 104863.
- [2] Hassam Ali, Muhammad Ali Muzammil, Dushyant Singh Dahiya, Farishta Ali, Shafay Yasin, Waqar Hanif, Manesh Kumar Gangwani, Muhammad Aziz, Muhammad Khalaf, Debargha Basuli, et al. 2024. Artificial intelligence in gastrointestinal endoscopy: a comprehensive review. *Annals of gastroenterology* 37, 2 (2024), 133.
- [3] Lei Cai, Jingyang Gao, and Di Zhao. 2020. A review of the application of deep learning in medical image classification and segmentation. *Annals of translational medicine* 8, 11 (2020), 713.
- [4] Xuanzhong Chen, Ye Jin, Xiaohao Mao, Lun Wang, Shuyang Zhang, and Ting Chen. 2026. Rareagents: Autonomous multi-disciplinary team for rare disease diagnosis and treatment. In *Proceedings of the AAAI Conference on Artificial Intelligence*, Vol. 40. 101–109.
- [5] Gheorghe Comanici, Eric Bieber, Mike Schaeckermann, Ice Pasupat, Naveen Sachdeva, Inderjit Dhillon, Marcel Blistein, Ori Ram, Dan Zhang, Evan Rosen, et al. 2025. Gemini 2.5: Pushing the frontier with advanced reasoning, multimodality, long context, and next generation agentic capabilities. *arXiv preprint arXiv:2507.06261* (2025).
- [6] Qianhan Feng, Zhongzhen Huang, Yakun Zhu, Xiaofan Zhang, and Qi Dou. 2025. UCAgents: Unidirectional Convergence for Visual Evidence Anchored Multi-Agent Medical Decision-Making. *arXiv preprint arXiv:2512.02485* (2025).
- [7] Google. 2025. Gemini-3. <https://gemini.google.com>. Official release version.
- [8] Peng Huang, Junhu Fu, Bowen Guo, Zeju Li, Yuanyuan Wang, and Yi Guo. 2025. VAP-Diffusion: Enriching Descriptions with MLLMs for Enhanced Medical Image Generation. In *International Conference on Medical Image Computing and Computer-Assisted Intervention*. Springer, 624–633.
- [9] Songhan Jiang, Fengchun Liu, Ziyue Wang, Linghan Cai, and Yongbing Zhang. 2026. PathReasoner-R1: Instilling Structured Reasoning into Pathology Vision-Language Model via Knowledge-Guided Policy Optimization. *arXiv preprint arXiv:2601.21617* (2026).
- [10] Lucie Joerg, Margaret Kabakova, Jennifer Y Wang, Evan Austin, Marc Cohen, Alana Kurti, and Jared Jagdeo. 2025. AI-generated dermatologic images show deficient skin tone diversity and poor diagnostic accuracy: an experimental study. *Journal of the European Academy of Dermatology and Venereology* 39, 12 (2025), 2134–2141.
- [11] Daniel Kermany. 2018. Large dataset of labeled optical coherence tomography (oct) and chest x-ray images. (*No Title*) (2018).
- [12] Hee E Kim, Alejandro Cosa-Linan, Nandhini Santhanam, Mahboubeh Jannesari, Mate E Maros, and Thomas Ganslandt. 2022. Transfer learning for medical image classification: a literature review. *BMC medical imaging* 22, 1 (2022), 69.
- [13] Jinhuk Lee, Wonjin Yoon, Sungdong Kim, Donghyeon Kim, Sunkyu Kim, Chan Ho So, and Jaewoo Kang. 2020. BioBERT: a pre-trained biomedical language representation model for biomedical text mining. *Bioinformatics* 36, 4 (2020), 1234–1240.
- [14] Qing Li, Weidong Cai, Xiaogang Wang, Yun Zhou, David Dagan Feng, and Mei Chen. 2014. Medical image classification with convolutional neural network. In *2014 13th international conference on control automation robotics & vision (ICARCV)*. IEEE, 844–848.
- [15] Tianwei Lin, Wenqiao Zhang, Sijing Li, Yuqian Yuan, Binhe Yu, Haoyuan Li, Wanggui He, Hao Jiang, Mengze Li, Xiaohui Song, et al. 2025. Healthgpt: A medical large vision-language model for unifying comprehension and generation via heterogeneous knowledge adaptation. *arXiv preprint arXiv:2502.09838* (2025).
- [16] Shengyuan Liu, Boyun Zheng, Wenting Chen, Zhihao Peng, Zhenfei Yin, Jing Shao, Jiancong Hu, and Yixuan Yuan. 2026. EndoBench: A comprehensive evaluation of multi-modal large language models for endoscopy analysis. *Advances in Neural Information Processing Systems* 38 (2026).
- [17] Yue Liu, Yunjie Tian, Yuzhong Zhao, Hongtian Yu, Lingxi Xie, Yaowei Wang, Qixiang Ye, Jianbin Jiao, and Yunfan Liu. 2024. Vmamba: Visual state space model. *Advances in neural information processing systems* 37 (2024), 103031–103063.
- [18] Ze Liu, Yutong Lin, Yue Cao, Han Hu, Yixuan Wei, Zheng Zhang, Stephen Lin, and Baining Guo. 2021. Swin transformer: Hierarchical vision transformer using shifted windows. In *Proceedings of the IEEE/CVF international conference on computer vision*. 10012–10022.
- [19] Zhuang Liu, Hanzi Mao, Chao-Yuan Wu, Christoph Feichtenhofer, Trevor Darrell, and Saining Xie. 2022. A convnet for the 2020s. In *Proceedings of the IEEE/CVF conference on computer vision and pattern recognition*. 11976–11986.
- [20] Omid Nejadi Manzari, Hamid Ahmadabadi, Hossein Kashiani, Shahriar B Shokouhi, and Ahmad Ayatollahi. 2023. MedViT: a robust vision transformer for generalized medical image classification. *Computers in biology and medicine* 157 (2023), 106791.
- [21] Yuren Mao, Wenyi Xu, Yuyang Qin, and Yunjun Gao. 2026. CT-Agent: a multimodal-LLM agent for 3D CT radiology question answering. *Science China Information Sciences* 69, 5 (2026), 150107.
- [22] OpenAI. 2024. ChatGPT. <https://chat.openai.com>. June 2024 version.
- [23] OpenAI. 2025. Introducing GPT-5. Web Page. <https://openai.com/zh-Hans-CN/index/introducing-gpt-5/>
- [24] Andre GC Pacheco, Gustavo R Lima, Amanda S Salomao, Breno Krohling, Igor P Biral, Gabriel G De Angelo, Fábio CR Alves Jr, José GM Esgario, Alana C Simora, Pedro BC Castro, et al. 2020. PAD-UFES-20: A skin lesion dataset composed of patient data and clinical images collected from smartphones. *Data in brief* 32 (2020), 106221.
- [25] Konstantin Pogorelov, Kristin Ranheim Randel, Carsten Griwodz, Sigrun Losada Eskeland, Thomas de Lange, Dag Johansen, Conchetto Spampinato, Duc-Tien Dang-Nguyen, Mathias Lux, Peter Thelin Schmidt, et al. 2017. Kvasir: A multi-class image dataset for computer aided gastrointestinal disease detection. In *Proceedings of the 8th ACM on Multimedia Systems Conference*. 164–169.
- [26] Qwen Team. 2026. Introducing Qwen3.5-Plus. Web Page. <https://qwen.ai/blog?id=qwen3.5>
- [27] Andrew Sellergren, Sahar Kazemzadeh, Tiam Jaroensri, Atilla Kiraly, Madeleine Traverse, Timo Kohlberger, Shawn Xu, Fayaz Jamil, Cían Hughes, Charles Lau, et al. 2025. Medgemma technical report. *arXiv preprint arXiv:2507.05201* (2025).
- [28] Sourabh Shastri, Isha Kansal, Sachin Kumar, Kuljeet Singh, Renu Popli, and Vibhakar Mansotra. 2022. CheXImageNet: a novel architecture for accurate classification of Covid-19 with chest x-ray digital images using deep convolutional neural networks. *Health and technology* 12, 1 (2022), 193–204.
- [29] Eric J Snider, Sofia I Hernandez-Torres, and Emily N Boice. 2022. An image classification deep-learning algorithm for shrapnel detection from ultrasound images. *Scientific reports* 12, 1 (2022), 8427.
- [30] Ismam Nur Swapnil, Aranya Saha, Tanvir Ahmed Khan, and Mohammad Ariful Haque. 2025. GRPO++: Enhancing Dermatological Reasoning under Low Resource Settings. *arXiv preprint arXiv:2510.01236* (2025).
- [31] Mingxing Tan and Quoc Le. 2021. Efficientnetv2: Smaller models and faster training. In *International conference on machine learning*. PMLR, 10096–10106.

¹<https://chat.openai.com>

- [32] Dongsheng Tian, Junzhe Jiang, Kai Zhang, Changchun Liu, Yu Yuan, Min Gao, and Enhong Chen. 2025. ECG-Doctor: An Interpretable Multimodal ECG Diagnosis Framework Based on Large Language Models. In *Proceedings of the 34th ACM International Conference on Information and Knowledge Management*. 2863–2873.
- [33] Petar Veličković, Guillem Cucurull, Arantxa Casanova, Adriana Romero, Pietro Lio, and Yoshua Bengio. 2017. Graph attention networks. *arXiv preprint arXiv:1710.10903* (2017).
- [34] Qin Wang, Zhiqing He, Yu Liu, Bowen Guo, Zeju Li, Miao Zhao, Wenhao Ju, Zhiling Luo, Xianhong Shu, Yi Guo, et al. 2026. EchoAgent: Towards Reliable Echocardiography Interpretation with "Eyes", "Hands" and "Minds". *arXiv preprint arXiv:2604.05541* (2026).
- [35] Yiming Xu, Qi Song, Yihan Wang, Wangqiu Zhou, and Junli Liang. 2025. LGC-CR: Few-shot Knowledge Graph Completion via Local Global Contrastive Learning and LLM-Guided Refinement. In *Proceedings of the 34th ACM International Conference on Information and Knowledge Management*. 3688–3697.
- [36] Jiancheng Yang, Rui Shi, Donglai Wei, Zequan Liu, Lin Zhao, Bilian Ke, Hanspeter Pfister, and Bingbing Ni. 2023. Medmnist v2-a large-scale lightweight benchmark for 2d and 3d biomedical image classification. *Scientific data* 10, 1 (2023), 41.
- [37] Yubiao Yue and Zhenzhang Li. 2024. Medmamba: Vision mamba for medical image classification. *arXiv preprint arXiv:2403.03849* (2024).
- [38] Hongbo Zhang, Junying Chen, Feng Jiang, Fei Yu, Zhihong Chen, Guiming Chen, Jianquan Li, Xiangbo Wu, Zhang Zhiyi, Qingying Xiao, et al. 2023. Huatuogpt, towards taming language model to be a doctor. In *Findings of the association for computational linguistics: EMNLP 2023*. 10859–10885.
- [39] Yuhang Zhang, Yiming Xu, Peilin Chen, Shiqi Wang, Qi Song, Lei Yu, and Wei Cai. 2025. Knowledge-enhanced medical image classification via descriptive priors from large language models. *Health Information Science and Systems* 13, 1 (2025), 61.
- [40] Shuaitao Zhao, Shijie Luo, Xinyuan Lu, and Weixiong Rao. 2025. MMKG-RAG: Retrieval-Augmented Generation with Multi-modal Knowledge Graph. In *International Conference on Database Systems for Advanced Applications*. Springer, 487–491.
- [41] Xianyao Zheng, Hong Yu, Hui Cui, Changming Sun, Xiangyu Li, Ran Su, Leyi Wei, Jia Zhou, Junbo Wang, and Qiangguo Jin. 2026. KG-CMI: Knowledge graph enhanced cross-Mamba interaction for medical visual question answering. *IEEE Transactions on Industrial Informatics* (2026).